Journal of Applied Electrochemistry **30**: 1043–1051, 2000.

Hypochlorite generation on Ru–Pt binary oxide for treatment of dye wastewater

C.-H. YANG[1], C.-C. LEE[1], T.-C. WEN[2]*
[1]*Department of Environmental and Chemical Engineering, Kung Shan University of Technology, Tainan 71016, Taiwan*
[2]*Department of Chemical Engineering, National Cheng Kung University, Tainan 71010, Taiwan*
*(*author for correspondence)*

Received 23 July 1999; accepted in revised form 12 April 2000

Key words: dye wastewater, hypochlorite production, Ruthenium–Platinum binary oxides

Abstract

Ruthenium–platinum binary oxides [$(Ru + Pt)O_x$] were coated on titanium substrates by thermal decomposition. The surface morphologies and elemental analyses of these electrodes were examined by means of scanning electron microscopy. The electrochemical behaviour was characterized by cyclic voltammetry (CV) and linear scanning voltammetry (LSV). The effects of electrolyte conditions on the current efficiency (CE) of hypochlorite production on binary $(Ru + Pt)O_x$ electrodes and the treatment of a high salt-containing dye wastewater using this hypochlorite were also investigated. The highest CE for hypochlorite production occurred on the RP1 (20 mol % Pt in precursor) electrode. The major factors influencing CE for hypochlorite production were the electrolyte flow rate, current density and chloride ion ($C1^-$) concentration. The RP1 electrode exhibited the best removal of organics and chromophoric groups in the dye wastewater. On this electrode, better removal of organics and chromophoric groups was obtained at 300 mA cm^{-2}. The colour of black–red dye wastewater became light yellow when a charge of 13.2 A h was passed while the COD of the wastewater decreased from 10 500 to 1250 mg L^{-1}.

1. Introduction

Metallic oxide coatings (DSA®) have been studied and successfully developed since 1969 [1, 2]. During 1968–1976, De Nora's research group [3, 4] started to investigate the use of DSA® as anode catalysts for the chlorine and oxygen evolution reactions. Later, many other metal oxide and their mixed-oxide electrodes were developed, for example, RuO_2, IrO_2, MnO_2, PtO_2, Co_3O_4, $NiCoO_4$ etc. [5].

Most transition metal oxides are stable in acidic or basic solution. In particular, platinum-family oxide electrodes possess the properties of high electrical conductivity, a porous surface and electrochemical catalytic activity [6]. Thermal decomposition [7–9] is the most popular method of preparing oxide electrodes due to its simplicity and reproducibility. The ruthenium oxide (RuO_2) electrode provides high catalytic activity for oxygen and chlorine evolution [10]. Unfortunately, RuO_2 produces RuO_4^{2-} or volatile RuO_4 [11] species during anodic polarization, leading to decline in the catalytical activity. To overcome this problem, a pure RuO_2 was mixed with a small amount of several inert metal oxides (e.g., TiO_2, ZrO_2, Ta_2O_5, SnO_2, PtO_x, IrO_2) [7, 8, 11–14], with the objective of maintaining high catalytic activity and stability.

Hypochlorite, an important oxidizing agent and mediator in water/wastewater treatment and organic synthesis, is formed from chlorine molecules in intermediate and basic solutions via: $Cl_2 + OH^- \rightleftharpoons HClO + Cl^-$ [15–17]. Thus, the development of electrocatalysts for this anodic process is an interesting topic. To obtain high CE, electrolytic preparation of hypochlorite is necessary to reduce energy-loss reactions [18].

Industrial wastewater usually contains organic pollutants which must be treated before the water can be discharged. Dye wastewater possesses colourful, high chloride-ion concentration and antibiologic organic (multibenzene ring compounds), which are very difficult to treat. Several processes have been applied for the removal of dye molecules from wastewater, either chemically or biologically or by a combination of the two [19–23]. With biological treatment, problems arise when water of high chloride content is discharged; thus pretreatment becomes mandatory. However, treatment with chemicals leads to the problem of excess reagent removal and the possible generation of side-products even more dangerous than the original pollutants. The electrochemical method for wastewater treatment has recently attracted attention [24], mainly because of the ease of operation and the increased efficiencies provided by the use of compact bipolar electrochemical reactors and by large surface area three dimensional electrodes.

In this work an attempt at mixing PtO_x and RuO_2 to increase electrode stability and promote oxygen

overpotential was made. Hypochlorite was produced on the $(Ru + Pt)O_x$ electrode. Furthermore, anodic oxidation of dye molecules in the wastewater was performed using the *in situ* produced hypochlorite.

2. Experimental details

2.1. *Electrode preparation*

Oxides of variable composition, X mol % Pt + $(100 - X)$ mol % Ru, were coated on a titanium substrate by thermal decomposition. The coating solution (precursor) contained a total concentration of 0.25 M H_2PtCl_6 (Johnson Matthey) and $RuCl_3$ (Johnson Matthey) in isopropanol (Merck GR) solution with 10% by volume concentrated HCl (Merck GR). The solutions were then repeatedly sonicated for 15 min periods in an ultrasonic bath (Branson Ultrasonic, connecticut). The titanium substrates were first degreased with soap and water, etched for 1h in a 6 M HCl solution at 80–90 °C, then washed with ultrapure water. After drying, the substrates were dipped in their respective isopropanol solution, dried in air for 30 min at room temperature and then dried at 85–90 °C in a vacuum furnace for 5–10 min at a reduced pressure of 400 mm Hg. The supports were then fired under air flow at 450 °C for 10 min. Further coatings were applied in a similar manner, a total of five being used in this work. The final annealing treatment in hot air at 450 °C took one hour. The freshly prepared electrodes were doubly coated with epoxy resin and PTFE films to provide suitable exposed geometric areas based on experimental requirement.

2.2. *Material characterization*

The surface morphologies/element analysis of the electrodes were examined by means of scanning electron microscopy (SEM) (Joel JSM35 SEM). The Auger electron spectroscopy (AES) measurements were performed using a Microlab 310D (VG Scientific) spectrometer. AES depth profiles were performed at emission currents of 0.1 and 8 mA with gun tension of 10 (electron) and 3 kV (ion), respectively.

2.3. *Electrochemical characterization*

The electrochemical properties of this series of Ru–Pt mixed oxide electrodes were examined by an electrochemical analyser system, BAS-100B (Bio-analytic System, USA). The electrochemical characteristics of the electrodes were examined by cyclic voltammetry and linear scanning voltammetry in a three-electrode cell. An Ag/AgCl electrode (Argenthal, 3 M KCl, 0.207 V vs SHE at 25 °C) was used as reference, while a platinum wire was employed as the counter electrode. A Luggin capillary, whose tip was set at a distance of about 1–2 mm from the surface of the working electrode, was used to minimize errors due to *IR* potential drop in the electrolytes. The potential was scanned at a rate of 50 mV s^{-1}, covering the 193 to 1220 mV potential range in 0.5 M H_2SO_4 and the −700 to 500 mV range in 1 M NaOH solution, respectively.

In addition, linear scanning voltammetry experiments for chlorine evolution were carried out in 3 M NaCl (Merck GR) and oxygen evolution in 1 M Na_2SO_4 (Merck GR), respectively. The potential sweep, at a scan rate of 1 mV s^{-1}, covered the 800 to 1500 mV potential range. All measurements were conducted at 25 °C using a thermostatically controlled water bath (Haake D8 and G).

2.4. *Hypochlorite preparation*

The hypochlorite production set-up comprised a Pyrex 'Jacket' cell which could be operated with or without flow (Figure 1), containing 500 mL 0.5 M NaCl. Hypochlorite was produced at 25 °C using a laboratory d.c. power supply (GPC-3030D, Good Will Instrument Company, Taiwan) in galvanostatic mode. The anode and cathode (Ti) were fixed at a distance of 3 cm with exposed geometric areas of 9 and 9.6 cm^2, respectively. Hypochlorite current efficiency was determined by the iodometric method [25] after passing of 3240 °C.

To investigate hypochlorite production in a flow system, the fractional factorial design method [26] was used to identify the key variables which influence current efficiency and energy yield from the following set of variables: (A) flow rate, (B) current density, (C) chloride ion concentration, and (D) electrode distance. Table 1

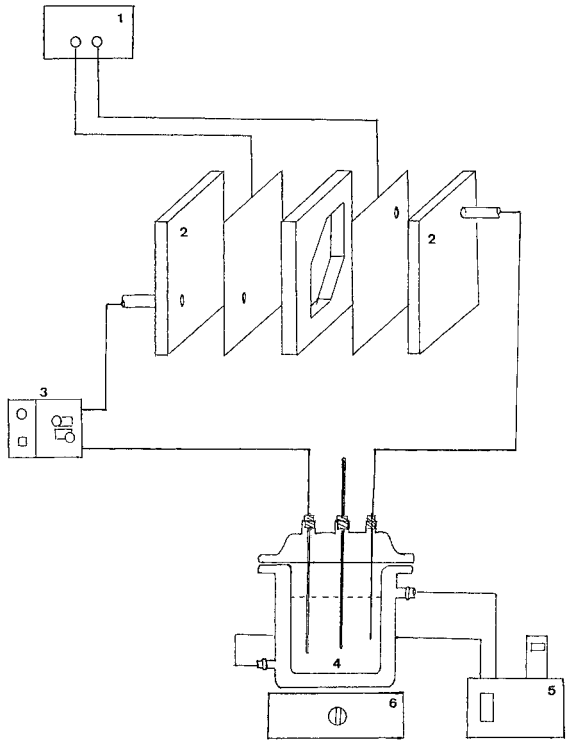

Fig. 1. Set-up for electrolytic generation of hypochlorite. Key: (1) d.c. power supply, (2) plate electrolysis cell, (3) pulse motor, (4) isothermal jacket cell, (5) temperature controller and (6) magnetic stirrer.

Table 1. Factors and levels for the 2^{4-1} fractional factorial design

Symbols	Factors	Levels	
		–	+
A	Flow rate/mL min^{-1}	130	400
B	Current density/mA cm^{-2}	300	500
C	Chloride (Cl^-) concentration/mol L^{-1}	0.5	1.0
D	Electrode distance/cm	0.45	0.65

gives the design factors and levels for the 2^{4-1} fractional factorial experiments which were employed. The results obtained are given in Table 2. The energy yield is defined as follows:

$$\text{Energy yield (g HClO/kWh)} = [\text{HClO}] \times V\left(\frac{IEt}{1000 \times 3600}\right)^{-1} \quad (1)$$

where [HClO] is the concentration of HClO (mg L^{-1}), V is the volume (L) of electrolytic solution, I is the applied current (A), E is the voltage (V) of electrolytic cell, and t is the electrolytic time (s).

2.5. *Electrolytic oxidation of dye wastewater*

The dye wastewater with high salt content was collected from a dye company in Tainan Hsien, Taiwan. The quality of this wastewater is given in Table 3. Chemical oxygen demand (COD), color and chloride ion concentration of the dye wastewater were determined by the potassium dichromate [25], u.v. absorbance spectrometer and the mercury nitrate method [25], respectively. A typical u.v. absorbance spectrum of this dye wastewater is shown in Figure 2. The wavelength of 542.5 nm in the visible region was used as the criterion of colour removal.

The set-up for dye wastewater (200 mL) treatment was the same as in Figure 1. The anode and cathode were fixed at a distance of 0.45 cm and had exposed geometric areas of 11 cm^2. The flow rate (130 mL min^{-1}) was controlled by an automotor (Waston–Marlow 302 S/RU) and the temperature was kept at 25 °C.

Table 2. Design matrix and experimental data from the 2^{4-1} fractional factorial design with the defining relation I = ABCD

Factors					Cell voltage /V	Current efficiency /%	Energy yield /g HClO $(kWh)^{-1}$
Run	A	B	C	D			
1	–	–	–	–	6.0	85.70	139.72
2	+	–	–	+	7.1	83.67	115.28
3	–	+	–	+	9.6	87.32	88.98
4	+	+	–	–	7.8	87.32	109.52
5	–	–	+	+	5.4	77.17	139.81
6	+	–	+	–	5.0	73.11	143.05
7	–	+	+	–	6.3	82.04	126.00
8	+	+	+	+	7.1	80.01	110.25

※ Anode: (Ru + Pt)O_x (20 mol % Pt)
Cathode: Ti
Temperature: 25 °C

Table 3. Quality of high salt-containing dye wastewater

Item	Analysis results
Colour	Black red
pH	6.5–7.0
COD/mg L^{-1}	11 000–12 000
Cl^-/mg L^{-1}	42 000–45 000
Electrical conductivity/S cm^{-1}	9×10^4–1.0×10^5
UV spectrum absorbance (×500):	
At 542.5 nm	0.504
At 519.5 nm	0.507

3. Results and discussion

3.1. *Characterization of (Ru + Pt)O_x electrode*

EDX was employed to detect elemental Pt distribution on the electrode surface. From the results shown in Figure 3, the Pt content on the electrode surface was found to increase with increasing Pt content in the coating solution and that Pt mole percent on the electrode surface was lower than that of the corresponding coating solution. The above observation is similar to that of Cominellis [27] on PtO_x derived from $H_2PtCl_6.5H_2O$. One possible explanation for this lower deposition yield is that part of the metal chloride is vaporized from the electrode surface at the temperature of calcination. The reaction between platinum and oxygen is incomplete during thermal decomposition resulting in the formation of nonstoichiometric PtO_x [28]. Thus, the Ru–Pt binary oxide electrodes are denoted as $(Ru + Pt)O_x$.

Figure 4 shows the SEM surface morphology of the $(Ru + Pt)O_x$ electrodes of RP1 and 40 mol % Pt (RP2) which exhibit white particles over the cracked surface.

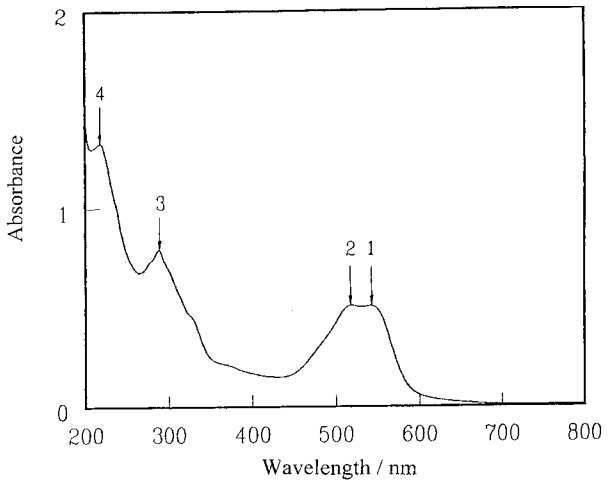

Fig. 2. Typical u.v. absorbance spectrum of high salt-containing dye wastewater. Key (wavelength/nm, absorbance): (1) 542.5, 0.504; (2) 519.5, 0.507; (3) 288.0, 0.791; (4) 218.5, 1.331.

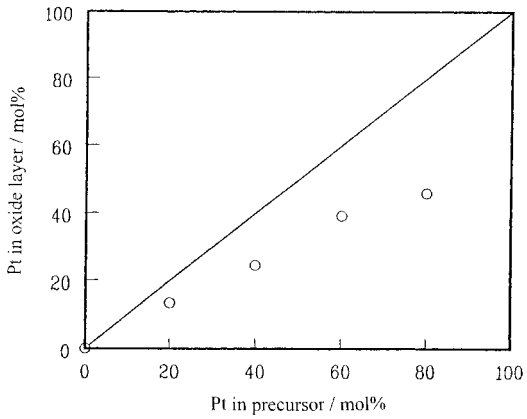

Fig. 3. Relationship of platinum content between precursor and electrode surface.

EDX was used to detect the composition of the white particles; results show that the compositions are Ru (31.78%), Ti (65.20%) and Pt (3.02%) for the RP1 electrode and Ru (54.24%), Ti (30.30%) and Pt (15.46%) for the RP2 electrode, respectively. In contrast, the electrode of 60 (RP3) and 80 mol% Pt (RP4) exhibited a smooth and dense surface.

To clarify the distribution of Pt and Ru oxides and depth profile of Pt, Ru, Ti and O within the coating matrix, Auger electron spectroscopy (AES) was used. The result obtained with the $(Ru + Pt)O_x$ electrode obtained by using 40 mol % Pt is shown in Figure 5. Curves 1, 2, 3 and 4 are indicative of Pt, Ru, O and Ti, respectively. The explanation for this result is as follows. Ruthenium dioxide may have migrated into the inner layer of the oxide coating and the titanium/oxide interface. This is due to the fact the crystalline structure of RuO_2 and TiO_2 is rutile [11]; accordingly, Pt is the surface enriched component. The O count gradually increases in the initial 10 ks, reaches a maximum at about 15 ks and decreases more quickly in the 20–25 ks region. In fact, most oxide coatings usually posses bulk oxygen deficient and surface oxygen excess phenomena because of the final annealing in air. The above result indicates that, during electrode preparation, several

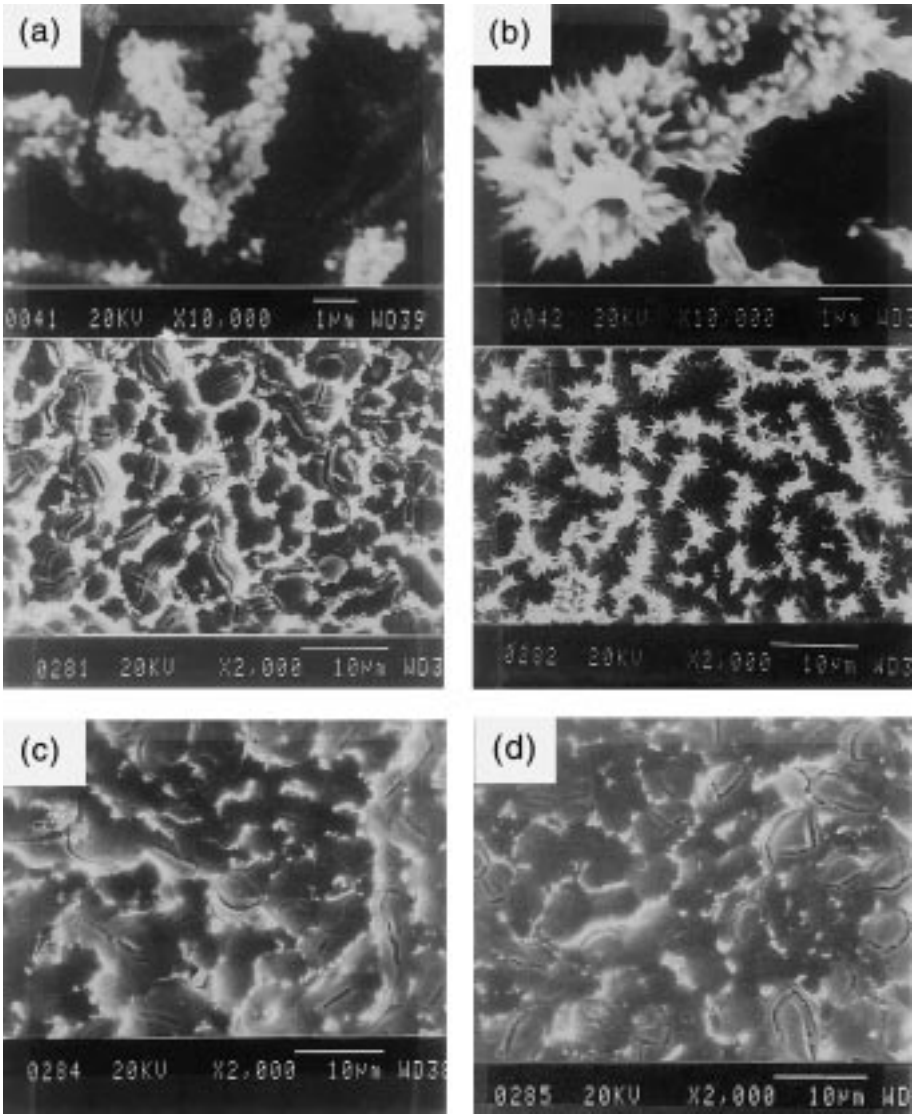

Fig. 4. SEM morphologies of (Ru + Pt) oxides with Pt content: (a) 20 (RP1); (b) 40 (RP2); (c) 60 (RP3) and (d) 80 (RP4) mol % in precursors.

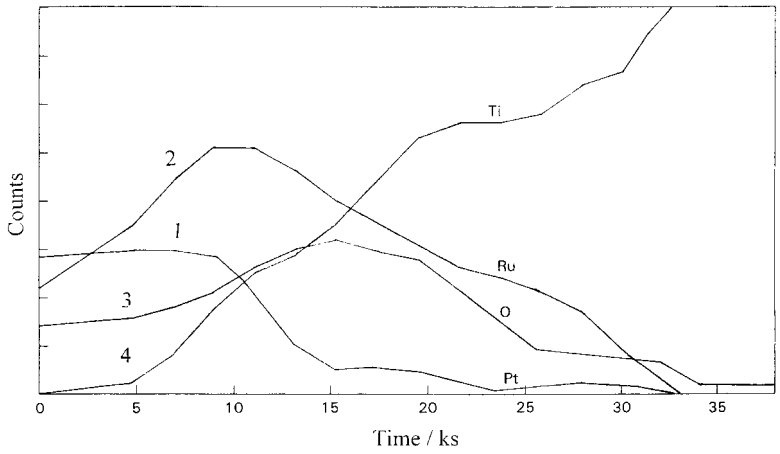

Fig. 5. An Auger depth profile of Ru, Pt, Ti and O from $(Ru + Pt)O_x$ electrode with 40 mol % Pt in precursor. The variable of time is proportional to the depth of emission, meanwhile the counts represent the relative distribution of these elements in this oxide film.

Pt(IV) atoms were reduced to PtO and Pt in the process of oxidation of isopropanol (precursor solvent) by Pt(IV) species, especially at higher temperatures [11].

Cyclic voltammograms of $(Ru + Pt)O_x$ in 0.5 M H_2SO_4 are shown in Figure 6. The background current increases with increasing Pt content. This result is attributable to the formation of a broad oxidation peak corresponding to PtO_x after 750 mV [9]. The peak corresponding to Ru(IV)/Ru(VI) is not clearly observed due to overlapping of the peak currents of the above process. A reduction peak at about 500 mV is attributable to the contribution of PtO_x reduction [27].

Cyclic voltammorgams of $(Ru + Pt)O_x$ electrodes in 1 M NaOH are shown in Figure 7. For a pure RuO_2 electrode, the redox couple at about 360 mV corresponds to the Ru(VI)/Ru(VII) transition [14]. This redox couple disappears while the PtO_x characteristic anodic (−200 mV) and cathodic (−350 mV) peaks appear. The background and reduction currents at −350 mV simultaneously increase with increasing Pt content. For the RP4 electrode, there are differences from the other three Pt-doped RuO_2 electrodes. Here, again, an oxidation peak at about 100 mV as well as a reduction peak at about −450 mV appear. The voltammetric curve of the RP4 electrode is similar to that of the $Ru_{0.3}$ $Pt_{0.4}$ $Ti_{0.3}$ O_x electrode [13]. The reduction peak at about −450 mV is related to the redox behaviour of Ru on the electrode surface; meanwhile, the broad oxidation peak at about 100 mV may arise from Pt oxidation or the high oxidation state of Ru on the electrode surface [13].

Voltammetric charge (q^*) [13, 14] is generally used as a criterion for measuring the active area of an oxide-coated electrode. In fact, an 'oxide' is often in the form of a hydrated oxide in aqueous solution [14, 29, 30]. The mechanism for redox transitions of the surface oxycations has been proposed as [14, 29, 30]:

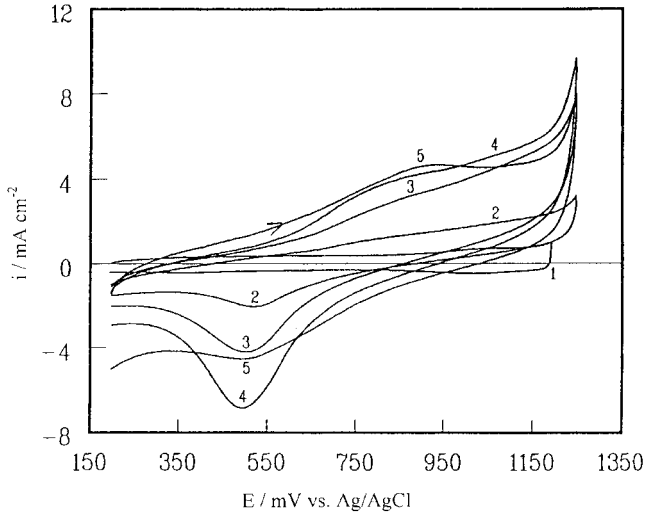

Fig. 6. Cyclic voltammograms in 0.5 M H_2SO_4 at a scan rate of 50 mV s^{-1} and 25 °C for $(Ru + Pt)O_x$ electrodes: (1) 0, (2) 20, (3) 40, (4) 60 and (5) 80 mol % Pt in precursors. Key: (1) RuO_2; (2) RP1; (3) RP2; (4) RP3 and (5) RP4.

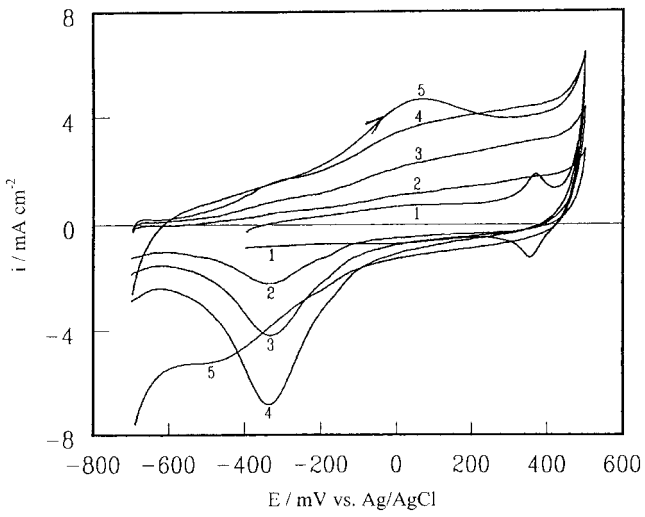

Fig. 7. Cyclic voltammograms in 1 M NaOH at a scan rate of 50 mV s^{-1} and 25 °C for $(Ru + Pt)O_x$ electrodes: (1) 0, (2) 20, (3) 40, (4) 60 and (5) 80 mol % Pt in precursors. Key: (1) RuO_2; (2) RP1; (3) RP2; (4) RP3 and (5) RP4.

$$[MO_a(OH)_b.xH_2O] + \delta H^+ + \delta e^- \rightleftharpoons [MO_{a-\delta}(OH)_{b+\delta}.xH_2O] \quad (2)$$

where surface oxycations exchange H (or OH) with the electrolyte solution when electron transfer occurs. The symbol, M, indicates a transition metal such as Ru, Ir, Ni, Co etc.

CV diagrams relating to H_2SO_4 and NaOH solutions for the Ru + Pt oxide electrode are presented in Figures 6 and 7, respectively. The voltammetric currents of these electrodes are not attributable to the redox transition of the surface oxyruthenium species, since these CV curves are different from that of RuO_2. This is due to the unstable (reducible) property of PtO_x, which is expected on repetitive potential cycling [31]. In previous work [32, 33], the oxidation and reduction on Pd metal reduced from PdO are much easier than on the normal bulk Pd and a similar result was reported in our other study [31]. Thus, the voltammetric currents on this mixed-oxide electrode are mainly due to Pt oxidation/reduction and hydrogen desorption/adsorption. In addition, the voltammetric response of this series of Ru + Pt oxide electrodes are similar in shape to those of PtO_x electrodes. These results reveal the instability of PtO_x. It is worth noting that oxides of platinum group metals are unstable in the hydrogen adsorption/desorption region [30]. This is supported by the CVs of the PtO_x and PdO_y electrodes. In contrast, RuO_2, IrO_2, RhO_2 and OsO_2 electrodes are quite stable under repetitive cycling between the oxygen and hydrogen evolving regions. In this study, q^* values were obtained by integrating the reduction current on the voltammetric curves in Figure 6 (in the range 193–1220 mV; 0.5 M H_2SO_4) and Figure 7 (in the range −600–500 mV; 1 M NaOH), respectively.

Figure 8 shows the plot of q^* against Pt content. It is clear that q^* increases with increasing Pt content. This suggests that change in surface morphology leads to an increase in effective area when Pt doped into (Ru + Ti)O_2. Though the SEM photographs (Figure 4) of the electrode surface exhibit many small white particles for the RP1 and the RP2 electrodes, the q^* values are still small. EDX analysis for these white particles reveals that Ru and Ti are major component with minor Pt content. Thus, these electrodes of low Pt contents possess lower q^*. With increasing Pt, the electrode surface appears smooth (Figure 4) in comparison with that for low Pt content and for these surfaces the surface area is not increased but q^* is very large. One possible explanation for this result is that the bonding between RuO_2 and nonstoichiometric PtO_x results in nonstoichiometric RuO_2 formation, leading to an increase in active sites on electrode surface.

Linear scan voltammograms (LSV) of chlorine evolution in 3 M NaCl on $(Ru + Pt)O_x$ electrodes are shown in Figure 9. A higher catalytic activity for chlorine evolution was noticed with $(Ru + Pt)O_x$ electrodes than RuO_2 electrode. Figure 10 gives the LSV of

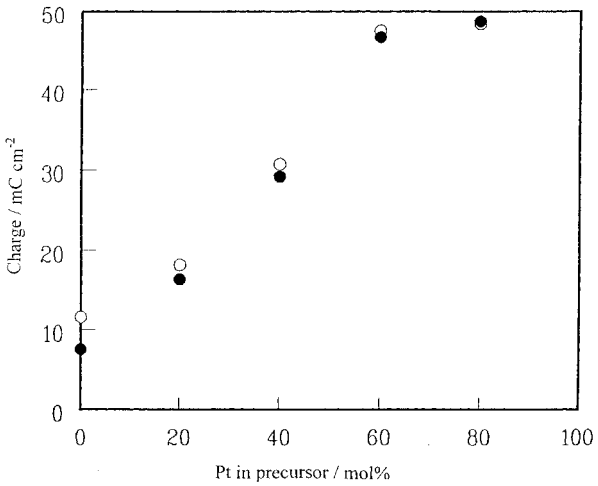

Fig. 8. Voltammograms charges of redox transition (q^*) for (Ru + Pt)O_x electrodes as a function of precursor Pt content in (○) 1 M NaOH and (●) 0.5 M H_2SO_4, at a scan rate of 50 mV s^{-1}.

oxygen evolution in 1 M Na_2SO_4 on $(Ru + Pt)O_x$ electrodes. The oxygen evolution, however, is inhibited on the RP1 and the RP2 electrodes. On the one hand, for the RP3 electrode a lower oxygen evolution was observed than that of RuO_2 electrode at a potential less than 1400 mV. On the other hand, a higher oxygen evolution was noticed than that of RuO_2 at potentials greater than 1400 mV. The catalytic activity of oxygen evolution is excellent on the RP4 electrode. These above results support that a RuO_2 electrode mixed with minor Pt content (<40 mol% Pt in precursor) inhibits oxygen evolution but increases catalytic activity of chlorine evolution; while a RuO_2 electrode mixed with high Pt content (>60 mol% Pt in precursor) increases the catalytic activity of both chlorine and oxygen evolutions.

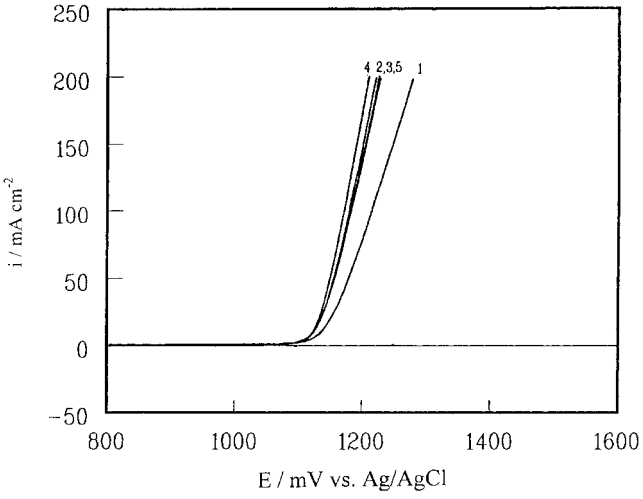

Fig. 9. Linear scanning voltammograms of chlorine evolution in 3 M NaCl at 1 mV s^{-1} for (Ru + Pt)O_x electrodes: (1) 0, (2) 20, (3) 40, (4) 60 and (5) 80 mol % Pt in precursors. Key: (1) RuO_2; (2) RP1; (3) RP2; (4) RP3 and (5) RP4.

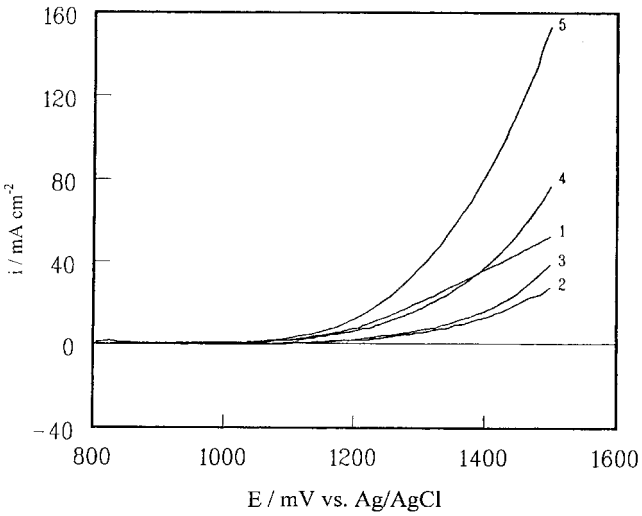

Fig. 10. Linear scanning voltammograms of oxygen evolution in 1 M Na_2SO_4 at 1 mV s^{-1} for $(Ru + Pt)O_x$ electrodes: (1) 0, (2) 20, (3) 40, (4) 60 and (5) 80 mol % Pt in precursors. Key: (1) RuO_2; (2) RP1; (3) RP2; (4) RP3 and (5) RP4.

3.2. *Electrolysis-generation of hypochlorite*

The current efficiency of hypochlorite production as a function of current density in 0.5 M NaCl on $(Ru + Pt)O_x$ electrodes is given Figure 11. Here, the current efficiency initially increases with increasing current density and thereafter decreases. The maximum current efficiency occurs at about 300 mA cm^{-2}. The current efficiency of $(Ru + Pt)O_x$ electrode is much higher than that of a pure RuO_2 electrode. It is important to note that the RP1 electrode possesses the highest current efficiency. However, as the Pt content in $(Ru + Pt)O_x$ electrodes increases, the current efficiency decreases (especially for the RP3 and the RP4 electrodes). These results support the interpretation given for the observations in Figures 9 and 10. The chlorine evolution activity on $(Ru + Pt)O_x$ electrodes in 3 M NaCl solutions remains the same. However, the oxygen evolution activity in 1 M Na_2SO_4 follows the order: RP4 > RP3 > RP2 > RP1 electrodes. This result is also consistent with the results on current efficiency of hypochlorite production.

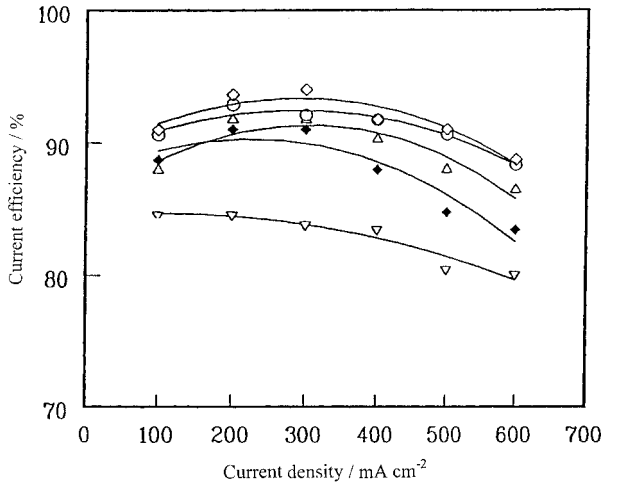

Fig. 11. Current efficiencies of $(Ru + Pt)O_x$ electrodes for hypochlorite production as a function of current density in 0.5 M NaCl solution. Platinum content: (▽, RuO_2) 0, (◇, RP1) 20, (○, RP2) 40, (△, RP3) 60 and (◆, RP4) 80 mol %.

3.3. *Effects of operation parameters on hypochlorite generation*

In practice, some operational parameters would influence both current efficiency and energy yield. From the above results, the best current efficiency for hypochlorite production occurred on the RP1 $(Ru + Pt)O_x$ electrode. Therefore, this electrode was concurrently selected as anode to perform batch flow experiments. The effects of the following parameters on the current efficiency and energy yield of hypochlorite production, respectively, were investigated: (A) flow rate (mL min^{-1}); (B) current density (mA cm^{-2}); (C) chloride ion concentration (mol L^{-1}); and (D) electrode distance (cm). In this study, 2^{4-1} fractional factorial design was utilized in designing these experiments.

The design factors and levels for the 2^{4-1} fractional factorial experiments are listed in Table 1 and the results of these experiments are given in Table 2. The level of each variable during a run is indicated in columns 2 to 5 of Table 2. The current efficiency and energy yield corresponding to each set of conditions are shown in column 6 and 7, respectively. Note that the combination of observations used in estimating the main effect of the factor D (electrode distance) is identical to that used for estimating the three-factor interaction effect of factors A (flow rate), B (current density), and C (chloride ion concentration). Hence, estimation of factor D and interaction effect of factors A, B, C and D are said to be 'confounded' [26]. Accordingly, the defining relation I = ABCD, suggested by Box et al. [26], was established in order to identify these relationships existing between these effects.

Estimation of the effects of experimental variables were algebraically made using the procedure recommended by Box et al. [26]. The results are presented in Table 4. Note that on employing the basic assumption of Box et al. [26], where higher order interaction effects (three and four-factor interactions in this study) are often neglected, the main and two factor interaction effects can be clearly obtained to result higher order interaction effects.

An examination of Table 4 reveals that effects of flow rate (A), current density (B) and chloride ion concentration (C) are the key variables influencing the current efficiency. The two factor interactions on the current efficiency are insignificant and do not require further interpretation. Thus, the effects of flow rate (A), current density (B) and chloride ion concentration (C) are discussed independently. Hence, an increase in the current efficiency corresponds to a decrease of flow rate (A), chloride ion concentration (C) and an increase of current density (B).

Table 4. Current efficiency and energy yield estimates of the effects from the 2^{4-1} fractional factorial design with the defining relation I = ABCD

Effects	Estimate	
	Current efficiency /%	Energy yield /g HClO $(kWh)^{-1}$
A + BCD	−2.03	−4.01
B + ACD	4.26	−25.78
C + ABD	−7.92	16.40
D + ABC	0.00	−15.99
AB + CD	1.02	6.50
AC + BD	−1.02	−2.15
AD + BC	1.63	2.47

※ Anode: (Ru + Pt)O_x (20 mol % Pt)

Table 4 shows that the effects of current density (B), chloride ion concentration (C) and electrode distance (D) are the key variables influencing the energy yield and that the two factor interactions on energy yield are insignificant. Subsequently, an increase in the energy yield corresponds to a decrease in current density (B), electrode distance (D) and an increase of chloride ion concentration (C).

3.4. *Treatment of high salt-containing dye wastewater*

From the above results, the effects of flow rate, current density and chloride ion concentration are shown to be the key variables influencing the current efficiency. While performing experiment on the electrolysis of high salt-containing dye wastewater, a low flow rate was maintained to promote current efficiency and also to decrease the electrode surface etching. Also, current density is an important factor in electrooxidation of wastewater as a consequence of the change of reaction on the electrode surface. Particularly, at high current density values, the wide changes in the driving force on an electrode surface can cause many possible reactions to occur. Therefore, the effects of current density on the removal of COD and colour from dye wastewater are primarily studied here.

The initial colour of dye wastewater was black–red, which subsequently changed during electrolysis into red, orange and finally to pale yellow. Also, as the dye wastewater consisted of surfactants suspended bubbles were be seen on the surface of dye wastewater. On application of 0.33 A h charge, the bubbles on the surface of dye wastewater were easily broken, indicating that the surfactants in the dye wastewater were decomposed under these conditions.

Current densities of 100, 300 and 500 mA cm^{-2}, respectively were used for the removal of COD and colour of the dye wastewater. The results of COD removal are presented in Figure 12 which shows that initial removal of COD at 300 and 500 mA cm^{-2} is faster than that at 100 mA cm^{-2}. The removal rate is reduced as the applied charge becomes larger than 5 A h.

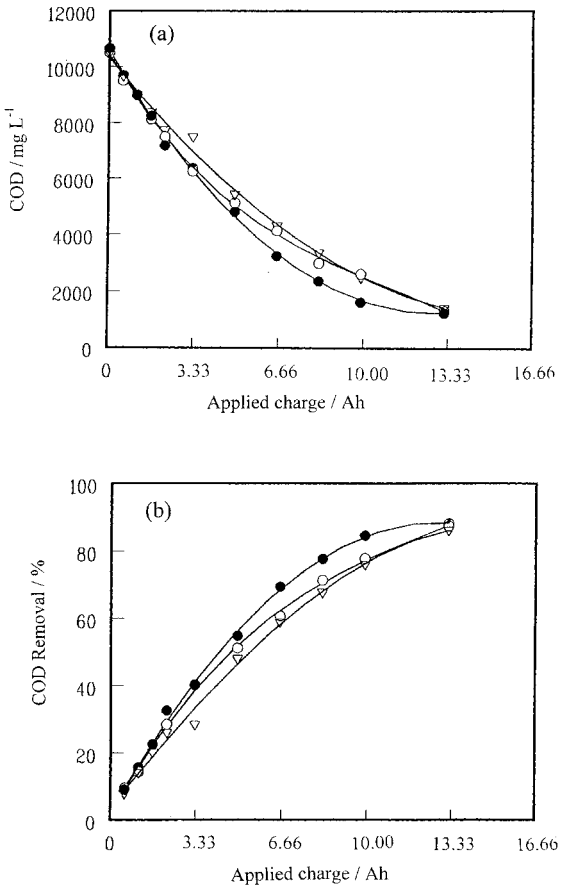

Fig. 12. COD removal of salt-containing dye wastewater against applied charge on (Ru + Pt)O_x electrode with 20 mol % Pt content. Applied current densities: (▽) 100, (○) 300 and (●) 500 mA cm^{-2}. Key: (a) COD residual and (b) COD removal rate.

For current density values beyond 100 mA cm^{-2}, a reduction in rate of COD removal was noticed. The COD removal rate for current densities of 100, 300 and 500 mA cm^{-2} were 86.30, 88.28 and 87.50%, respectively, with a total applied charge of 13.2 A h. This type of slow-down phenomenon of the COD removal rate was noticed specifically in the final stages of electrolysis with high hypochlorite concentration. This can be explained by the difficulty in oxidizing the organics and the decrease in decomposition rate as the residual COD decreases. In total, the best COD removal efficiency occurred at 300 mA cm^{-2}. This is consistent with the results on current efficiency of electrogenerated hypochlorite (see previous Section).

Dye wastewater possesses an obvious colour, which has attracted many researchers to remove the colour. Here, u.v. absorption spectrometer was employed to detect the colour removal. Prior to analysis, the sample of dye wastewater was suitably diluted with distilled water. The absorbance changes at the wavelength of 542.5 nm were taken as the criterion of colour removal. Figure 13 shows the results. This electrooxidation method for the colour removal is shown to be an efficient process. With an applied charge of 1.1 A h, the absorbance at 542.4 nm becomes almost zero. At this

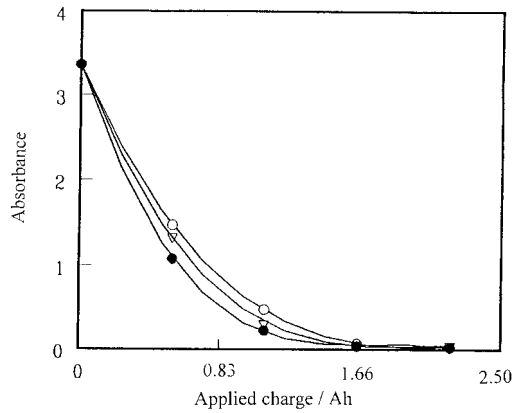

Fig. 13. Colour removal of salt-containing dye wastewater against applied charge on $(Ru + Pt)O_x$ electrodes with 20 mol % Pt content. The u.v. absorbance at 542.5 nm was employed as the criterion of colour removal. Applied current densities: (▽) 100, (○) 300 and (●) 500 mA cm^{-2}.

time, the colour of wastewater (black–red) became transparent orange. The color removal efficiency had the following order with respect to current density: $300 > 100 > 500$ mA cm^{-2} . This result also supports the higher current efficiency of hypochlorite production at 300 mA cm^{-2}.

4. Conclusions

The addition of PtO_x to RuO_2 electrodes results in an increase in nonstoichiometric number, which leads to an increase in the active area of electrode. The q^* value, activity of chlorine and oxygen evolution increases with increasing Pt content. The q^* value of 60–80 mol% Pt electrodes is four times higher than that of a pure RuO_2 electrode. With $(Ru + Pt)O_x$ binary electrodes, the best current efficiency for hypochlorite production occurred with 20 mol% Pt electrode. A higher current efficiency for hypochlorite production was obtained under the following conditions: low flow rate (130 mL min^{-1}), high current density (500 mA cm^{-2}) and low chloride ion concentration (0.5 mol L^{-1}). A higher energy yield was obtained under the following conditions: low current density (300 mA cm^{-2}), high chloride ion concentration (1 mol L^{-1}) and electrode distance (0.45 cm). The COD was reduced and the colour of high salt-containing dye wastewater were removed with ease using the oxidation of electrogenerated hypochlorite ions. With an applied charge of 13.2 A h, COD was reduced from 10,500 to 1250 mg L^{-1} with a removal efficiency of 88%, during which the black-red dye wastewater was changed into pale yellow.

Acknowledgement

Partial financial support of this work by the National Science Council of Taiwan, Kung Shan Institute of Technology and National Cheng Kung University is acknowledged. The technical English consultation by Dr A. Gopalan is also acknowledged.

References

1. H. Beer, *US Patent 3 632 498* (1972).
2. H. Beer, *US Patent 3 711 385* (1973).
3. G. Bianchi, V. DeNora, P. Gallone and A. Nidola, *US Patent 3 616 445* (1971).
4. G. Bianchi, V. DeNora, P. Gallone and A. Nidola, *US Patent 3 948 751* (1971).
5. S. Trasatti, 'Electrodes of Conductive Metallic Oxides, Part B' (Elsevier, Amsterdam, 1981), pp. 627–59.
6. R. Seyd, J. Orehotsky, W. Visscher and S. Srinivasan, *J. Electrochem. Soc.* **129** (1982) 1990.
7. G. Battaglin, A. Carnera, P. Mazzoldi, G. Lodi, P. Bonora, A. Eaghetti and S. Trasatti, *J. Electroanal. Chem.* **135** (1982) 313.
8. L.D. Burke and M. McCarthy, *Electrochim. Acta* **29** (1984) 211.
9. S. Trasatti, 'Electrodes of Conductive Metallic Oxides. Part A' (Elsevier, New York, 1980), pp. 146–52.
10. S.M. Lin and T.C. Wen, *J. Electrochem. Soc.* **140** (1993) 2265.
11. F. Hine, M. Yasuda and T. Yoshid, *J. Electrochem. Soc.* **124** (1977) 500.
12. C. Iwakura and K. Sakamoto, *J. Electrochem. Soc.* **132** (1985) 2420.
13. T.A.F. Lassali, J.F.C. Boodts, S.C. DeCastro, R. Landers and S. Trasatti, *Electrochim. Acta* **38** (1993) 95.
14. T.C. Wen and C.C. Hu, *J. Electrochem. Soc.* **139** (1992) 2158.
15. J.A. Harrison, D.L. Caldwell and R.E. White, *J. Electrochem. Soc.* **29** (1983) 1561.
16. J.A. Harrison, D.L. Caldwell and R.E. White, *J. Electrochem. Soc.* **29** (1984) 203.
17. G.H. Kelsall, *J. Appl. Electrochem.* **14** (1984) 177.
18. R.E. Buys and T.D. Reynolds, Proc. 36th Industrial Waste Conference, Purdue University (1981), p. 29.
19. D.W. Wertter and A.G. Hodgson, Proc. 32nd Industrial Waste Conference, Purdue University (1977), p. 1.
20. G.H. Davis, J.H. Koon and C.E. Adam, Proc. 32nd Industrial Waste Conference, Purdue University (1977), p. 981.
21. J.L. Mahloch, A. Slindala, E.C. McGriff, Jr. and W.A. Barnett, Proc. 29th Industrial Waste Conference, Purdue University (1974) p. 44.
22. E. Gilbert, *Water Sci. & Technol.* **14** (1982) 849.
23. D. Zhou, M.W. Cai and W.Q. Hui, *Water Sci. & Technol.* **19** (1987) 391.
24. L.C. Chiang, J.E. Chang and T.C. Wen, *Water Res.* **29** (1995) 671.
25. 'Standard Methods for the Examination of Water and Wastewater', APHA 16th edn (1985), p. 426.
26. G.E.P. Box, W.G. Hunter and J.S. Hunter, 'Statistics for Experiments', (J. Wiley & sons, New York, 1978), pp. 374–433.
27. C. Comninellis and G.P. Vercesi, *J. Appl. Electrochem.* **21** (1991) 136.
28. M.E.G. Lyons and L.D. Burke, *J. Chem. Soc., Faraday Trans. 1*, **83** (1987) 299.
29. L.D. Burke and O.J. Murphy, *J. Electroanal. Chem.* **96** (1979) 19.
30. S. Trasatti, *op. cit.* [9], p. 301.
31. C.C. Hu and T.C. Wen, *J. Electrochem. Soc.* **14** (1995) 1376.
32. C.C. Hu and T.C. Wen, *Electrochim. Acta* **40** (1995) 495.
33. T.C. Wen and C.C. Hu, *J. Electrochem. Soc.* **140** (1993) 998.